# Stability of active suspensions

Christel Hohenegger* and Michael J. Shelley

*Courant Institute of Mathematical Sciences, New York University, 251 Mercer Street, New York, New York 10012, USA*
(Received 26 May 2009; revised manuscript received 25 January 2010; published 20 April 2010)

We study theoretically the stability of "active suspensions," modeled here as a Stokesian fluid in which are suspended motile particles. The basis of our study is a kinetic model recently posed by Saintillan and Shelley [D. Saintillan and M. J. Shelley, Phys. Rev. Lett. **100**, 178103 (2008); D. Saintillan and M. J. Shelley, Phys. Fluids **20**, 123304 (2008)] where the motile particles are either "pushers" or "pullers." General considerations suggest that, in the absence of diffusional processes, perturbations from uniform isotropy will decay for pullers, but grow unboundedly for pushers, suggesting a possible ill-posedness. Hence, we investigate the structure of this system linearized near a state of uniform isotropy. The linearized system is nonnormal and variable coefficient, and not wholly described by an eigenvalue problem, in particular at small length scales. Using a high wave-number asymptotic analysis, we show that while long-wave stability depends on the particular swimming mechanism, short-wave stability does not and that the growth of perturbations for pusher suspensions is associated not with concentration fluctuations, as we show these generally decay, but with a proliferation of oscillations in swimmer orientation. These results are also confirmed through numerical simulation and suggest that the basic model is well-posed, even in the absence of translational and rotational diffusion effects. We also consider the influence of diffusional effects in the case where the rotational and translational diffusion coefficients are proportional and inversely proportional, respectively, to the volume concentration and predict the existence of a critical volume concentration or system size for the onset of the long-wave instability in a pusher suspension. We find reasonable agreement between the predictions of our theory and numerical simulations of rodlike swimmers by Saintillan and Shelley [D. Saintillan and M. J. Shelley, Phys. Rev. Lett. **99**, 058102 (2007)].

## I. INTRODUCTION

Swimming mechanisms for self-locomoting microorganisms range from flagellar rotation [1], to ciliary and tail beating [1,2], to actin-tail polymerization [3,4]. Recently, locomotion of artificial microswimmers, activated say by chemical reactions [5–7] or an external magnetic field [8–11], has also been demonstrated. These swimming modes have the common feature that a self-propelling particle exerts a propulsive force on the fluid which must be balanced by the fluid drag. The hydrodynamics of motile suspensions, in which many such microorganisms or artificial swimmers create large-scale flows, has received much attention in recent years. Of particular interest are the formations of large-scale vortices and jets reported by Kessler and co-workers [12–15] for fairly concentrated bacterial baths. These flow features have been reproduced qualitatively in simulations of Hernández-Ortiz and co-workers [16,17] using a simple swimming dumbbell model that includes only far-field hydrodynamics, as well as in simulations of more complicated models of rodlike swimmers by Saintillan and Shelley [18]. To study such phenomenon in a continuum setting, Saintillan and Shelley [19,20] developed a continuum theory for the dynamics of a dilute suspension of active rodlike particles in which fluid motions are driven by the "extra stress" generated by each particle's induced far-field flow. This model is closely related to classical models of rigid rod suspensions [21] and generalizes a phenomenological model of swimming suspensions by Simha and Ramaswamy [22]. Saintillan and Shelley showed, for rear-actuated swimmers, the existence of a long-wave instability to the isotropic state, and nonlinear two-dimensional simulations showed that these instabilities drove the system to a strong mixing dynamics with features again qualitatively similar to experiment. Most recently, Baskaran and Marchetti [23] posed a coarse-grained, in part phenomenological, hydrodynamic model for active suspensions and classified various long-range isotropic and nematic instabilities. Subramanian and Koch [24] gave essentially the same model as Saintillan and Shelley but included the additional effect of run-and-tumble dynamics of the swimmers.

The goal of this paper is to study the general stability of an isotropic and uniform suspension of active swimmers. We consider two broad categories: pushers and pullers. A pusher is a swimming particle whose motion is actuated along the posterior of the body, while for a puller, motion is actuated along the anterior. These two actuation modes result in oppositely signed extra-stress contributions to the fluid. Bacteria such as *B. subtilis*, used by Kessler and co-workers in their studies [12–15], are pushers, while algae-like *Chlamydomonas*, when "rowing" with their leading flagella, are pullers. This distinction is by no means exclusive, as certain highly symmetric organisms such as spherical multicellular algae (e.g., *Volvox*) may fall between the pusher-puller distinction, as would densely covered ciliates. For our model, the uniform, isotropic state is a natural one to study, as it provides the state of minimum configurational entropy, and an entropy equality predicts that for pusher suspensions, there will be an increase in fluctuations. In part, it is the nature of these fluctuations that we seek to study. In our

*choheneg@cims.nyu.edu

analysis, we will focus (to a degree) on dynamics in the absence of diffusive mechanisms, particularly rotational. The mechanisms by which diffusion might arise are various—pair interactions, run-and-tumble dynamics, thermal fluctuations—and so this aspect is less universal, though certainly important, than bare hydrodynamic interactions. Further, understanding the creation of fine-scale structure in the absence of diffusive effects is important to understanding basic model well-posedness as well as the actual effects of diffusion.

First, in Sec. II, we review the active suspension model of Saintillan and Shelley. It is comprised of a Smoluchowsky equation whose configuration variables are active particle center-of-mass and orientation and whose fluxes for translation and rotation are driven by a background velocity field, single-particle locomotion, and diffusional processes. The velocity (and its gradients) is determined by a Stokes fluid equation forced by the active particles' extra stress. In Sec. III, we derive the Smoluchowsky equation linearized about uniform isotropy. We show that system instability can only arise from the dynamics of the first azimuthal mode in swimmer orientation, itself described by an integral equation in polar angle, that perturbations can only grow for suspensions of pushers, and that concentration fluctuations are generically bounded. Shelley and Saintillan [19,20] examined stability by solving the eigenvalue problem for exponential growth and showed the existence of a long-wave instability for pushers. We recapitulate that study and show further that, in the absence of rotational diffusion, solutions to the eigenvalue problem only exist for a finite range of wave numbers with the loss of solutions associated with an emerging singularity in the associated eigenfunction. Hence, the eigenvalue problem does not address stability at intermediate and small length scales. To partially study this, we develop a high wave-number asymptotic treatment for the linearized equations, showing that at small scales the system is well-behaved independently of the nature of the suspension. This construction shows that the growth of perturbations for pusher suspensions is associated not with concentration fluctuations, as these are generally bounded or decay, but with a proliferation of oscillations in swimmer orientation. We confirm our basic results through numerical simulations. We demonstrate also that the addition of rotational diffusion to the eigenvalue problem apparently removes the singular behavior at intermediate length scales.

Finally, in Sec. IV, we relate our study to previous work, particularly the swimming particle simulations of Saintillan and Shelley [18] and recent experiments of Sokolov *et al.* [25]. In the former, the authors observed at low volume concentration that the dimensional rotational and translational diffusion coefficients are proportional and inversely proportional to the volume concentration, respectively. In this case, we predict the existence of a critical volume concentration and find reasonable agreement with their simulations. The same analysis predicts a critical system size above which a pusher suspension is unstable and below which it is stable. Our analysis predicts critical lengths smaller than that reported by Sokolov *et al.* [25], though the experiment has several complicating factors, such as possible oxygen taxis by the swimmers.

## II. KINETIC MODEL

We study a continuum model describing the dynamics of a dilute suspension of self-propelled rodlike particles (see Saintillan and Shelley [19,20]). Each particle is described by two configuration variables: its center-of-mass position **x** and orientation vector **p** ($\mathbf{p} \cdot \mathbf{p} = 1$). Without any other flow effects, each particle swims along its axial direction **p** and generates in the fluid a force dipole (stresslet) $\sigma_0(\mathbf{pp} - \mathbf{I}/3)$. Saintillan and Shelley [19,20] noted that $\sigma_0$ can be related to the swimming velocity $U_0$ by $\sigma_0 / U_0 \mu l^2 = \alpha$, where $l$ is the characteristic length of the swimmer, $\mu$ is the viscosity of the suspending fluid, and $\alpha$ is a $O(1)$ dimensionless geometric constant which differentiates between pullers ($\alpha > 0$) and pushers ($\alpha < 0$). A pusher swims by an actuating stress along the posterior of the body, resulting in a negative force dipole on the fluid, while a puller swims by an actuating stress along the anterior, resulting in a positive force dipole on the fluid (see also Hernández-Ortiz *et al.* [16], Ishikawa and Pedley [26], Underhill *et al.* [17], and Kanevsky *et al.* [27]).

Let $\Psi(\mathbf{x}, \mathbf{p}, t)$ be the time-dependent probability distribution function associated with the configuration variables **x** and **p**. $\Psi$ evolves by the conservation (Smoluchowski) equation

$$\frac{\partial \Psi}{\partial t} = -\nabla_x \cdot (\dot{\mathbf{x}} \Psi) - \nabla_p \cdot (\dot{\mathbf{p}} \Psi), \tag{1}$$

where the nondimensional particle fluxes are

$$\dot{\mathbf{x}} = \mathbf{p} + \mathbf{v} - D\nabla_x(\ln \Psi), \tag{2}$$

$$\dot{\mathbf{p}} = (\mathbf{I} - \mathbf{pp})(\nabla_x \mathbf{v} \, \mathbf{p}) - d\nabla_p(\ln \Psi). \tag{3}$$

Equation (2) for the position flux $\dot{\mathbf{x}}$ consists of three terms: the self-locomotion velocity along the orientation direction **p**, the background velocity **v** induced by the other swimmers, and the center-of-mass diffusion where $D$ is the translational diffusion coefficient. Equation (3) is Jeffery's equation for the rotation of a rod by a linear flow [28], including rotational diffusion with diffusion coefficient $d$. Here, $\nabla_p$ is the gradient on the surface of the unit sphere $S$, $\nabla_x$ is the gradient in Cartesian coordinates, and spatially periodic boundary conditions are assumed. Finally, the normalization of $\Psi$ is chosen as $\frac{1}{V} \int dS_p \int dV_x \Psi = 1$, where $V$ denotes the fluid volume in a cube of length $L$ and $\Psi_0 = 1/4\pi$ is the probability density for the uniform isotropic state. Here, velocity has been scaled on swimmer velocity $U_0$ and length on the intrinsic length $l_c = \nu^{-1}l$, where $\nu$ is the relative swimmer volume concentration $\nu = Nl^3/L_p^3$, with $N$ the total number of swimming particles in the system of dimensional volume $L_p^3$ [note that Shelley and Saintillan [18] used $\tilde{\nu} = N(l/2)^3/L_p^3 = \nu/8$ as their definition]. Hence, $L = L_p/l_c$ is the dimensionless system size.

Assuming low Reynolds number flow, as is characteristic of the locomotion of small organisms, the fluid velocity **v** is found by balancing the Newtonian fluid stress against the active stress produced by the swimming particles

$$\nabla_x q - \Delta_x \mathbf{v} = \nabla_x \cdot \boldsymbol{\Sigma}^a \quad \nabla_x \cdot \mathbf{v} = 0, \tag{4}$$

where $q$ is the fluid pressure. The active stress tensor $\boldsymbol{\Sigma}^a$ is expressed as the distributional average of single-particle stresses over orientations $\mathbf{p}$,

$$\boldsymbol{\Sigma}^a = \alpha \int dS_p \Psi(\mathbf{x}, \mathbf{p}, t)(\mathbf{pp} - \mathbf{I}/3) \tag{5}$$

(see Batchelor [29] and Saintillan and Shelley [19,20]). It is the choice of the intrinsic length scale $l_c$ that leaves only the parameter $\alpha$ in Eq. (5).

When diffusional processes are absent, the system Eqs. (1)–(5) has several interesting aspects: (i) the swimmer concentration $\nu$ appears only through the normalized system size $L = L_p/l_c$; (ii) if $t$ and $\mathbf{x}$ are rescaled as $(\mathbf{x}, t) \rightarrow (\mathbf{x}, t)/|\alpha|$, then up to its sign, $\alpha$ can be scaled out of the dynamics and so only the cases $\alpha = \pm 1$ need be considered; and (iii) if $\alpha < 0$, then the dynamics for $\alpha > 0$ is gotten by simply reversing time, orientation, and velocity, i.e., $(t, \mathbf{p}, \mathbf{v}) \rightarrow -(t, \mathbf{p}, \mathbf{v})$. This reflects the reversibility of the single microswimmer. Rotational or translational diffusion destroys this symmetry.

Equations (1)–(5) form the dynamical system we will study. It is nearly identical to classical theories of the dynamics of rigid rod suspensions [21], with the exceptions being that for passive rigid rods, $\alpha$ is always positive and there is no single-rod velocity term $\mathbf{p}$ in Eq. (2). As in classical rod theory, the relative configurational entropy, $\mathcal{S} = \int dV_x \int dS_p \frac{\Psi}{\Psi_0} \ln \frac{\Psi}{\Psi_0}$, is a natural measure of system fluctuations. It is nonnegative and only attains its minimum at zero for $\Psi = \Psi_0$. Further, it obeys the evolution equation [20]

$$\Psi_0 \dot{\mathcal{S}} = -\frac{3}{\alpha} \int dV_x \int dS_p \mathbf{E} : \mathbf{E}$$

$$- \int dS_p \int dV_x [D|\nabla_x \ln \Psi|^2 + d|\nabla_p \ln \Psi|^2]\Psi, \tag{6}$$

where $\mathbf{E} = \frac{1}{2}(\nabla_x \mathbf{v} + \nabla_x \mathbf{v}^T)$ is the symmetric rate-of-strain tensor. The first term on the right-hand side is proportional to the rate of viscous dissipation. Diffusional processes give the second term, which is strictly negative and serves to drive $\mathcal{S}$ toward its minimum. Hence, for suspensions of pullers, where $\alpha > 0$, we have $\dot{\mathcal{S}} < 0$ and fluctuations away from the uniform isotropic state ($\Psi = \Psi_0$) are expected to decay. On the other hand, for pushers ($\alpha < 0$), the leading term is now positive, which allows the possibility of fluctuation growth and eventual balance with diffusion. This is observed in simulation where strongly mixing flows emerge through a growth of fluctuations from near isotropy and which are eventually balanced, though only on average, by diffusion [19,20]. If there is no diffusional processes and $\alpha < 0$, Eq. (6) predicts that fluctuations will grow.

## III. LINEAR STABILITY ANALYSIS

We study the stability of the system under small perturbations from uniform isotropy. Hence, let $\Psi = \frac{1}{4\pi}(1 + \varepsilon \psi)$, where $\int dV_x \int dS_p \psi = 0$, $\mathbf{v} = \varepsilon \mathbf{u}$, and $q \rightarrow \epsilon q$, with $\varepsilon \ll 1$. Keeping only linear-order terms, Eqs. (1)–(5) become

$$\psi_t + \mathbf{p} \cdot \nabla_x \psi - 3\mathbf{pp} : \nabla_x \mathbf{u} = D\nabla_x^2 \psi + d\nabla_p^2 \psi, \tag{7}$$

$$- \Delta_x \mathbf{u} + \nabla_x q = \nabla_x \cdot \boldsymbol{\Sigma} \quad \nabla_x \cdot \mathbf{u} = 0, \tag{8}$$

with $\boldsymbol{\Sigma} = (\alpha/4\pi) \int dS_p \psi(\mathbf{pp} - \mathbf{I}/3)$. Here we have used the equality

$$\nabla_p \cdot (\mathbf{I} - \mathbf{pp})\nabla_x \mathbf{u}\, \mathbf{p} = -3\mathbf{p} \cdot \nabla_x \mathbf{u}\, \mathbf{p} = -3\mathbf{pp} : \nabla_x \mathbf{u},$$

which follows from the identity $\nabla_p(f_1 \hat{\theta} + f_2 \hat{\phi}) = (1/\sin \phi)[\partial_\theta f_1 + \partial_\phi(\sin \phi f_2)]$ and $\nabla_x \cdot \mathbf{u} = 0$.

This system can be much simplified. Equations (7) and (8) have five degrees of freedom: three in space and two in orientation. The first step of the stability analysis is to transform the equations through a spatial Fourier transform $\mathcal{F}_x$ in $\mathbf{x}$ and decouple Eqs. (7) and (8) according to the wave vector $\mathbf{k}$ ($k = |\mathbf{k}|$). Here, $\tilde{f}_k = \mathcal{F}_x[f] = \int dV e^{-i\mathbf{k} \cdot \mathbf{x}} f(\mathbf{x})$, where $\mathbf{k} = (2\pi/L)\mathbf{k}'$ and $\mathbf{k}' \in \mathbb{Z}^3$. From Eq. (8), with $\mathbf{k} = k\hat{\mathbf{k}}$, we have $\tilde{\mathbf{u}}_k = (i/k)(\mathbf{I} - \hat{\mathbf{k}}\hat{\mathbf{k}})\tilde{\boldsymbol{\Sigma}}_k \hat{\mathbf{k}}$ and Eq. (7) then becomes

$$\partial_t \tilde{\psi}_k = -ik\hat{\mathbf{k}} \cdot \mathbf{p}\, \tilde{\psi}_k - Dk^2 \tilde{\psi}_k + d\nabla_p^2 \tilde{\psi}_k - 3\mathbf{pp} : (\mathbf{I} - \hat{\mathbf{k}}\hat{\mathbf{k}})\tilde{\boldsymbol{\Sigma}}_k(\hat{\mathbf{k}}\hat{\mathbf{k}}). \tag{9}$$

The explicit dependence of Eq. (9) on the direction of $\hat{\mathbf{k}}$ can be removed by a change of variables: $\mathbf{p} = \mathbf{R}\hat{\mathbf{q}}$, where $\mathbf{R}$ is the rotation matrix so that $\hat{\mathbf{k}} = \mathbf{R}\hat{\mathbf{z}}$ and $\hat{\mathbf{q}} = (\cos \theta \sin \phi, \sin \theta \sin \phi, \cos \phi)$, with $\theta \in [0, 2\pi]$ the azimuthal angle and $\phi \in [0, \pi]$ the polar angle on the unit sphere. With these definitions, Eq. (9) becomes

$$\partial_t \tilde{\psi}_k = -ik \cos \phi \tilde{\psi}_k - Dk^2 \tilde{\psi}_k + d\nabla_q^2 \tilde{\psi}_k$$

$$- 3 \cos \phi \hat{\mathbf{q}} \cdot (\mathbf{I} - \hat{\mathbf{z}}\hat{\mathbf{z}})\mathbf{R}^T \tilde{\boldsymbol{\Sigma}}_k \mathbf{R}\hat{\mathbf{z}}. \tag{10}$$

To simplify Eq. (10), we note that

$$\hat{\mathbf{q}} \cdot (\mathbf{I} - \hat{\mathbf{z}}\hat{\mathbf{z}})\mathbf{R}^T \tilde{\boldsymbol{\Sigma}}_k \mathbf{R}\hat{\mathbf{z}}$$

$$= \frac{\alpha}{4\pi} \sin \phi \hat{\mathbf{e}}(\theta) \cdot \int_0^{2\pi} d\theta' \hat{\mathbf{e}}(\theta')$$

$$\times \int_0^\pi d\phi'\, \tilde{\psi}_k(\theta', \phi', t)\sin^2 \phi'\, \cos \phi',$$

where $\hat{\mathbf{e}}(\theta) = \cos \theta \hat{\mathbf{x}} + \sin \theta \hat{\mathbf{y}} + 0\hat{\mathbf{z}}$.

While Eqs. (7) and (8) decoupled under a Fourier transform in $\mathbf{x}$, Eq. (10) retains a variable coefficient structure in $\phi$. A further decoupling in $\theta$ is achieved by introducing a Fourier series expansion in $\theta$: $\tilde{\psi}_k = \Sigma_n A_{n,k}(\phi, t)e^{in\theta}$. After some algebra, we find

$$\partial_t A_{n,k} + A_{n,k}(ik \cos \phi + Dk^2)$$

$$+ d\left(\frac{n^2}{\sin^2 \phi}A_{n,k} - \frac{1}{\sin \phi}\partial_\phi(\sin \phi \partial_\phi A_{n,k})\right)$$

$$= -\frac{3\alpha}{4}\cos \phi \sin \phi F[A_{n,k}]\delta_{n,1}, \tag{11}$$

where the scalar $F$ operator is

$$F[h] = \int_0^\pi d\phi' h(\phi') \sin^2 \phi' \cos \phi'$$

and $\delta_{n,1}$ is the Kronecker delta symbol. As a technical aside, note that $\widetilde{\psi}_k$ becomes uniform in $\theta$ as $\phi \to 0, \pi$, implying that $A_{n,k}(0,t) = A_{n,k}(\pi,t) = 0$ for $n \neq 0$.

The main feature of Eq. (11) is that the extra-stress contribution (involving the operator $F$) arises only in the dynamics of the $n=1$ azimuthal mode. As we now show, the remaining modes yield only temporal decay or saturation.

The expanded entropy $\mathcal{S}$ yields the squared $L^2$ norm of the perturbation $\psi$: $\mathcal{S} = \varepsilon^2 \mathcal{S}_2 + O(\varepsilon^3)$, where $\mathcal{S}_2 = \frac{1}{2}\int dV_x \int dS_p \psi^2$ and

$$\dot{\mathcal{S}}_2 = -\frac{3}{\alpha}\int dV_x \nabla_x \mathbf{u} : \nabla_x \mathbf{u} - D\int dV_x \int dS_p |\nabla_x \psi|^2$$
$$- d\int dV_x \int dS_p |\nabla_p \psi|^2. \qquad (12)$$

The Plancherel and Parsevaal theorems then yield

$$\mathcal{S}_2 = \pi \sum_{k,n}\int_0^\pi d\phi' \sin \phi' |A_{n,k}(\phi',t)|^2 = \frac{1}{2}\sum_{k,n}\|A_{n,k}(\cdot,t)\|^2_{L^2(S)}.$$

A straightforward substitution and integration by parts show that for the $n=1$ azimuthal mode

$$\frac{d}{dt}\|A_{1,k}(\cdot,t)\|^2_{L^2(S)}$$
$$= -3\pi\alpha|F[A_{1,k}]|^2$$
$$- 4\pi D\int_0^\pi d\phi' \sin \phi |A_{1,k}(\phi',t)|^2$$
$$- 4\pi d\int_0^\pi d\phi' \sin \phi \left(|\partial_\phi A_{1,k}(\phi',t)|^2 + \frac{|A_{1,k}(\phi',t)|^2}{\sin^2 \phi'}\right). \qquad (13)$$

Here, the only potential source of growth in this mode is the extra-stress contribution when $\alpha < 0$, i.e., for pushers. For $\alpha > 0$, the right-hand side is negative definite and the mode will decay. We study in Sec. III B the $n=1$ mode at large $k$.

For the other azimuthal modes ($n \neq 1$), a very similar calculation yields

$$\frac{d}{dt}\|A_{n,k}(\cdot,t)\|^2_{L^2(S)}\begin{cases}<0 & \text{for } d>0 \text{ and/or } D>0 \\ =0 & \text{for } d=D=0\end{cases} \qquad (14)$$

and hence these contributions to the $L^2$ norm decay or are invariant in time. This is unsurprising: if $d=0$ and $n \neq 1$, the exact solution of Eq. (11) is $A_{n,k}(\phi,t) = A_{n,k}(\phi,0)e^{-(ik\cos \phi + Dk^2)t}$.

Finally, consider the swimmer concentration field $c = \int dS_p \Psi$ for which $c = 1 + \varepsilon c_1 + O(\varepsilon^2)$ with $c_1 = \frac{1}{4\pi}\int dS_p \psi$. Hence,

$$\widetilde{c}_{1k}(t) = \frac{1}{2}\int_0^\pi d\phi' \sin \phi' A_{0,k}(\phi',t). \qquad (15)$$

Applying the Hölder inequality gives $|\widetilde{c}_{1k}(t)| \leq 2\pi\|A_{0,k}(\phi,t)\|_{L^2(S)}$ and since by Eq. (14) the upper bound is strictly decaying for $d \neq 0$, $|\widetilde{c}_{1k}(t)|$ is trapped in a decaying envelope. Hence, for the linearized system and independently of the sign of $\alpha$, concentration fluctuations do not grow. Saintillan and Shelley [19,20] also reached this conclusion based on the form of eigenfunctions associated with the more restricted eigenvalue problem, which we now re-examine.

### A. Eigenvalue problem

The first approach to study stability, following Saintillan and Shelley [19,20], is to make an exponential ansatz for the solutions of Eq. (11). Only the first azimuthal mode with $\alpha < 0$ is of interest and we focus on the special case when $D = d = 0$ and $\alpha < 0$ (pushers)

$$\partial_t A_{1,k} + ik\cos \phi A_{1,k} = -\frac{3\alpha}{4}\cos \phi \sin \phi F[A_{1,k}]. \qquad (16)$$

Hence, assume that $A_{1,k}(\phi,t) = \gamma_k(\phi)e^{\sigma t}$. There is no *a priori* expectation that $A_{1,k}$ can be represented in this fashion as Eq. (16) is variable coefficient in $\phi$. Indeed, we will see that eigenvalues exist only for a finite range of $k$ and other approaches are necessary to understand stability more generally. Note that if $\alpha < 0$, then the dynamics for $\alpha > 0$ is gotten by reversing time ($t \to -t$) and reflecting $\phi$ across the equator ($\phi \to \pi - \phi$) in Eq. (16). Consequently, if $\sigma$ is an eigenvalue for some $\alpha < 0$, then $-\sigma$ is an eigenvalue for $-\alpha$. Rotational diffusion destroys this symmetry, while translational diffusion is accounted for trivially by shifting $\sigma$ down by $Dk^2$.

Inserting the ansatz into Eq. (16) gives

$$\gamma_k(\phi) = -\frac{3\alpha \cos \phi \sin \phi}{4(\sigma + ik\cos \phi)}F[\gamma_k]. \qquad (17)$$

Applying $F$ to both sides then yields the eigenvalue relation

$$-\frac{3}{4}\alpha \int_0^\pi d\phi' \frac{\sin^3 \phi' \cos^2 \phi'}{\sigma + ik\cos \phi'} = 1. \qquad (18)$$

To evaluate this complex-valued integral, let $u = \cos \phi$ and separate into real and imaginary parts. Some algebra produces the complex equation

$$-\alpha\left[4i\sigma k^3 + 6i\sigma^3 k - 3\sigma^2(\sigma^2 + k^2)\ln\frac{\sigma + ik}{\sigma - ik}\right] = 4ik^5, \qquad (19)$$

where the complex logarithm is defined as $\ln(a+ib) = \ln\sqrt{a^2 + b^2} + i\arctan\frac{b}{a}$. Note that Eq. (19) is only valid if $\text{Re}(\sigma) \neq 0$. Figure 1 shows the numerical solution of Eq. (19), plotting the real and imaginary parts of $\sigma$ for $\alpha = -1$. For small $k$, there are two branches of unstable eigenvalues with zero imaginary part. These two branches fuse into a single unstable branch, now with an imaginary component, with the decrease of growth rate suggesting a crossing of the
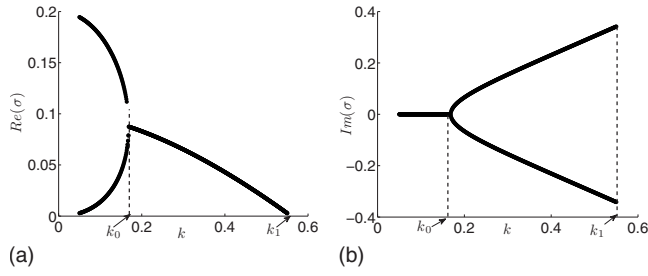
FIG. 1. Real and imaginary parts of the growth rate $\sigma(k)$ for $\alpha = -1$ (pushers) with $D = d = 0$.

$k$ axis to become negative. Saintillan and Shelley [20] gave the asymptotic solution in $k \ll 1$ for the upper branch in Fig. 1

$$\sigma(k) = -\frac{\alpha}{5} + \left[ \frac{15}{7\alpha} - D \right] k^2 + O(k^3). \quad (20)$$

For a suspension of pushers ($\alpha < 0$), Eq. (20) implies the existence of a long-wave instability with $\lim_{k\to 0}\sigma(k) = -\alpha/5 > 0$. In contrast, for Pullers, there is no long-wave instability and perturbations will generically decay as we argue in the previous sections.

We now examine the eigenvalue problem more deeply. Let $k_1$ be the value of $k$ where $\sigma$ approaches zero growth rate and $k_0$ be the first value of $k$ where the two branches become one (see Fig. 1). Having solved $\sigma(k)$ for $k < k_1$ in Eq. (19) and using that $F[\gamma_k]$ is a function of time only, the spatial structure of the corresponding eigenvector $\gamma_k$ in Eq. (17) is given by

$$u_k(\phi) = -\frac{3\alpha \cos \phi \sin \phi}{4[\sigma(k) + ik \cos \phi]}.$$

The real part of $u_k(\phi)$ for $k = 0.2$, 0.4, 0.5 and $\mathrm{Im}(\sigma) > 0$ is plotted in Fig. 2(a). As $k \to k_1$, a singularity in $u_k$ develops around $\phi \approx 2.2$. The eigenfunctions are the same for $\mathrm{Im}(\sigma) < 0$, but reflected across the equator. To understand this singular behavior, as well as the overall branch structure, we
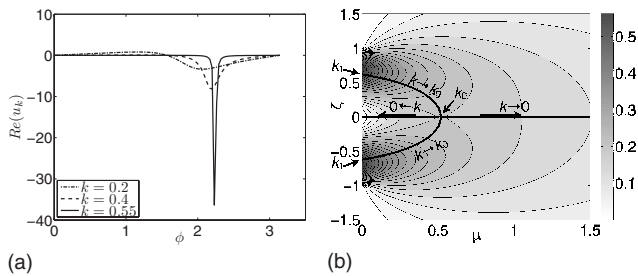


FIG. 2. (a) Real part of the eigenvector $u_k(\phi)$ for $k = 0.2$, 0.4, 0.55, with $\alpha = -1$ (pushers) and $D = d = 0$. Note the nearly singular structure for $k$ slightly below $k_1 \approx 0.56$. (b) Contour plots of the imaginary part of the left side of Eq. (21) as a function of $\mu, \zeta$ (maximum value $\approx 0.56$). The intersection of the $(\mu, \zeta)$ surface with the $k$ planes and the contour line of the real part of Eq. (21) (thick black) give the solution set of Eq. (19). Arrows follow the bifurcation diagram.

rescale Eq. (19) in terms of the real and imaginary parts, setting $\lambda = \sigma/k = \mu + i\zeta$,

$$
\begin{aligned}
f(\mu,\zeta) + ig(\mu,\zeta) = -\frac{\alpha}{4}\Bigg\{ & 4i(\mu + i\zeta) + 6i(\mu + i\zeta)^3 \\
& - 3(\mu + i\zeta)^2[(\mu + i\zeta)^2 + 1] \\
& \times \left[ \frac{1}{2}\ln\frac{\mu^2 + (\zeta+1)^2}{\mu^2 + (\zeta-1)^2} + i\arctan\frac{\zeta+1}{\mu} \right. \\
& \left. - i\arctan\frac{\zeta-1}{\mu} \right] \Bigg\} = ik.
\end{aligned} \quad (21)
$$

Since $\arctan x^{-1}$ is not a continuous function at $x = 0$, Eq. (21) implies the existence of a discontinuity in $\mu(k)$ as $\mu$ goes through zero. For a suspension of pushers ($\alpha < 0$), the long-wave asymptotics of Eq. (20) guarantees that for $k < k_1$, $\mu$ is positive. Thus, $k_1$ is obtained by taking the limit of the left side of Eq. (21) as $\mu$ decreases to zero

$$\left[ -4\zeta + 6\zeta^3 - 3\zeta^2(\zeta^2 - 1)\ln\frac{|\zeta+1|}{|\zeta-1|} - 3i\pi(\zeta^4 - \zeta^2) \right] = 4ik_1. \quad (22)$$

We find that $k_1 \approx 0.5597$ and $\zeta_1 \approx 0.6232$.

Taking the limit of the left side of Eq. (21), as $\mu$ increases to zero, changes the minus sign before the last term on the left side of Eq. (22) and the resulting equation has no solution for $k_1$. Therefore, the curve $\mathrm{Re}(\sigma)$ in Fig. 1(a) cannot be continued past $k_1$.

In Fig. 2(b), we plot the contour lines of $g(\mu,\zeta)$, the imaginary part of the left side of Eq. (21) and the zero-level curves of $f(\mu,\zeta)$, the real part (thick black line). In the rescaled coordinates $\mu, \zeta$, the solutions $\sigma(k) = k\lambda(k)$ of Eq. (19) are found by simultaneously satisfying $f(\mu,\zeta) = 0$ and $g(\mu,\zeta) = k$. The maximum value of $g$ is $k_1$ and it is attained for the purely imaginary solutions $\lambda(k_1) = \pm i\zeta_1$. Hence, there are no solutions for $k > k_1$. As $k$ decreases, the solution $\lambda(k)$ moves from $\lambda(k_1)$ along the level curves $f(\mu,\zeta) = 0$ toward their intersection with the real axis at the saddle point of $g$ at height $k_0$. From there, two real branches emerge as $k$ is further decreased toward zero. The branch to the left goes to the origin where $g$ reaches a minimum of zero and corresponds to the lower branch in Fig. 1(a). Recalling that $\mu/k = \mathrm{Re}(\sigma)$, the right branch, characterized by $\mu \to \infty$ and $k \to 0$, yields the upper branch in Fig. 1(a). This can be formally shown by an asymptotic expansion similar to the one yielding Eq. (20). The arrows in Fig. 2(b) follow the bifurcation diagram as $k$ decreases to zero. Note that since the values of $g$ are negative for $\mu < 0$, there can be no intersection between $g$ and the $k$ plane in the second and third quadrants. Hence, the solution to the eigenvalue problem Eq. (18) exists only for the finite range of wave numbers $0 \leq k < k_1$. Thus, the set of eigenvectors cannot describe general solutions of the linearized problem and, in particular, does not give information on smallscale behavior, important for well-posedness. Furthermore, since we find an apparently finite number of branches, an arbitrary initial perturbation cannot be decomposed into a linear combination of eigenfunctions. Note that the same singular behavior in eigenfunctions is observed for pullers ($\alpha$

$> 0$) as $\mu$ *increases* toward zero.

Note that if $k = k_1$ indeed marks a point of stability transition (though the eigenvalue problem has no solution for $k > k_1$), then one concludes immediately that there exists a critical system size $L_p$ or volume concentration $\nu$ above which the system becomes unstable. This follows from having scaled on the intrinsic length $l_c$, so that $\mathbf{k} = (2\pi/L)\mathbf{k}' = (2\pi l)/(\nu L_p)\mathbf{k}'$, with $\mathbf{k}' \in \mathbb{Z}^3$. Hence, $k_1' = (k_1/2\pi)(\nu L_p/l)$. As the first allowable mode in the periodic box has $k' = 1$, the system is unstable if $k_1' \approx 0.089(\nu L_p/l) > 1$ and is stable otherwise. For negative $\alpha \neq -1$, the instability condition becomes $0.089(|\alpha|\nu L_p/l) > 1$. We will consider the effect of diffusion shortly.

### B. Large $k$ analysis of the first azimuthal mode

To gain a more general understanding, we now consider the asymptotic behavior of the first azimuthal mode ($n = 1$) in Eq. (16) for large $k$. We will show that for $k$ large and independently of $\alpha$, the solutions develop a proliferation of oscillations under a fixed envelope. After some algebraic manipulations, Eq. (16) may be rewritten as

$$C_t(x,t) = -\frac{3\alpha}{4}h(x)e^{iktx}\int_{-1}^{1}C(y,t)e^{-ikty}dy, \qquad (23)$$

where $x = \cos\phi$, $h(x) = x^2(1-x^2)$, and $C(x,t) = \sqrt{h(x)}e^{iktx}A_{1,k}(x,t)$. Upon extending $C$ and $h$ to zero outside $[-1,1]$, Eq. (23) becomes in Fourier space

$$\widetilde{C}_t(\omega,t) = -\frac{3\alpha}{4}\widetilde{h}(\omega - kt)\widetilde{C}(kt,t). \qquad (24)$$

Next, we integrate Eq. (24) with respect to time, letting $\omega = kt$ and $b(t) = \widetilde{C}(kt,t)$,

$$b(t) = \widetilde{C}(kt,0) - \frac{3\alpha}{4}\int_0^t \widetilde{h}[k(t-s)]b(s)ds. \qquad (25)$$

That is, we have reduced the stability question to analysis of a scalar integral equation in one variable. Since $h(x)$ is zero outside $[-1,1]$, its Fourier transform can be computed. It satisfies $\lim_{\omega \to 0}\widetilde{h}(\omega) = 4/15$ and $\widetilde{h}(\omega)$ is $O(\omega^{-2})$ for $\omega \gg 1$.

We now consider the asymptotic limit where $k$ is large and $t$ is fixed and we show that the integral in Eq. (25) decays like $O(k^{-2})$ and thus $b(t)$ is essentially determined by $\widetilde{C}(kt,0)$. To achieve this, we transform Eq. (25) to Laplace space and use the convolution and shift theorems to get

$$\mathcal{L}[b](r) = \frac{\mathcal{L}[\widetilde{C}(kt,0)](r)}{1 + \dfrac{3\alpha}{4k}\mathcal{L}[\widetilde{h}](r/k)},$$

$$\text{where} \qquad \mathcal{L}[\widetilde{h}](r) = r\int_{-1}^{1}\frac{h(x)}{r^2+x^2}dx. \qquad (26)$$

The complex-valued integral in Eq. (26) can be evaluated by separating the real and imaginary parts and for $k$ large, its leading-order behavior is $(4r)/(3k)$. Therefore, the behavior of the Laplace transform becomes
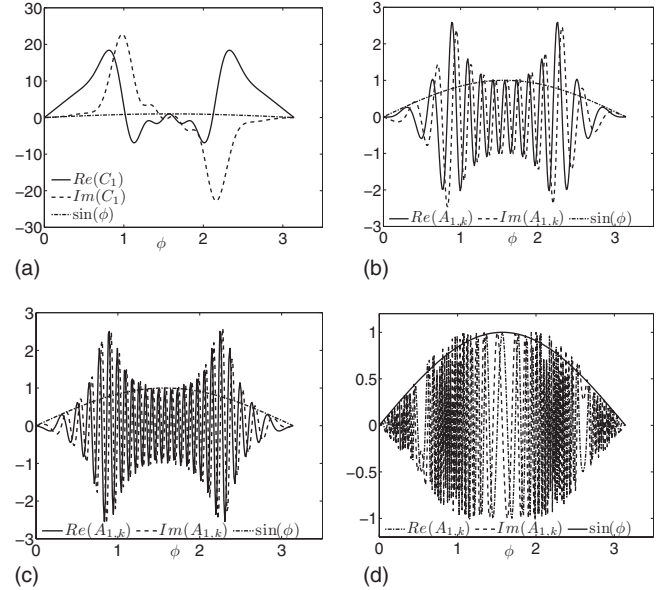


FIG. 3. Real and imaginary parts of first Fourier modes $A_{1,k}(\phi,t)$ for $\alpha = -1$ (pushers) and $D = d = 0$ from a single mode sinusoid initial condition. The increasing wave numbers $k$ show growth (upper left), saturation with an increasing number of oscillations in time (upper right, bottom left), and convergence of the wave envelope to that of the initial condition.

$$\mathcal{L}[b](r) \approx \mathcal{L}[\widetilde{C}(kt,0)](r)\frac{1}{1 + \alpha r/k^2}$$

$$\approx \mathcal{L}[\widetilde{C}(kt,0)](r)\left(1 - \alpha\frac{1}{k}\frac{r}{k}\right) \quad \text{for } k \text{ large.}$$

Since $\mathcal{L}[\widetilde{C}(kt,0)](r)$ also scales like $g(r/k)/k$ for some function $g$, the reminder term in the previous approximation is $O(k^{-2})$ and $\mathcal{L}[b](r) \approx \mathcal{L}[\widetilde{C}(kt,0)](r)$.

Back substitution to $A_{1,k}(\phi,t)$ then gives

$$A_{1,k}(\phi,t) \approx e^{-ikt\cos\phi}A_{1,k}(\phi,0) \qquad (27)$$

for $k$ large and $t$ fixed. This analysis shows that solutions of Eq. (16) for $k$ large exhibit an oscillatory behavior independently of $\alpha$ and its sign. The envelope is given by the initial condition and the number of oscillations increases with $t$. Finally, numerical simulations (see Sec. III C) show that for values of $k$ in between the exponential growth and the large $k$ analysis, solutions for $t$ large are of the form

$$A_{1,k}(\phi,t) \approx e^{-ikt\cos\phi}A_{1,k}(\phi,t_*),$$

where $t_*$ corresponds to the time at which the transition from growth to saturation occurs.

### C. Numerical simulations

We simulate Eq. (16) with a second-order Crank-Nicolson scheme. First, we consider a single sinusoidal initial condition $A_{1,k}(\phi,0) = \sin(\phi)$ and recalling the analysis of Secs. III A and III B, we neglect diffusion and set $d = D = 0$. In Fig. 3, the real and imaginary parts of $A_{1,k}$ for $k = 0.4$, $k = 0.8$, and $k = 10$ are plotted at $t = 50$ and $t = 100$ for pushers ($\alpha = -1$). For
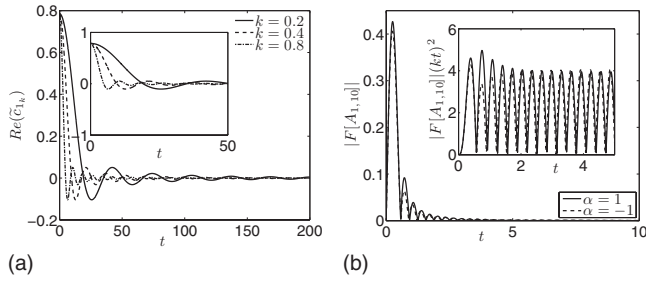
FIG. 4. Starting from a single initial sinusoidal wave with $d=D=0$ and for pushers ($\alpha=-1$). (Left) Evolution of $\text{Re}[\widetilde{c}_{1k}(t)]$ for various $k$; (inset) short-time evolution. (Right) Evolution of $|F[A_{1,10}]|$; (inset) $|F[A_{1,10}]|(kt)^2$.

$k=0.4$, the real and imaginary parts [Fig. 3(a)] are growing as would be predicted by the eigenvalue analysis. The values $k=0.8$ and $k=10$ are out of the range of exponential growth and both real and imaginary parts of the solution show oscillations with constant $L^2(S)$ norm (see also Fig. 6). The number of oscillations increases with time as illustrated in Figs. 3(b) and 3(c), and Fig. 3(d) shows that for $k$ large, the envelope of the oscillations is determined by the initial condition.

Next, Fig. 4 illustrates the time evolution of both $\text{Re}[\widetilde{c}_{1k}]$ and $|F[A_{1,k}]|$, again starting from a single sinusoidal wave, in the absence of any diffusion. The time evolution of $\widetilde{c}_{1k}$, the Fourier transform of the linearized concentration, is shown in Fig. 4(a) together with an inset showing the short-time behavior. As expected, fluctuations in the linearized concentration decay to zero for all Fourier modes. The time evolution of $|F[A_{1,k}]|$ for $k=10$ and both pullers ($\alpha=1$) and pushers ($\alpha=-1$) in Fig. 4(b) together with the inset where $|F[A_{1,k}]|$ is multiplied by $(kt)^2$ confirm that for $k$ large, $|F[A_{1,k}]|$ decays to zero like $(kt)^{-2}$. Thus, the small-scale behavior is independent of $\alpha$ and its sign as predicted in Sec. III B.

The influence of the rotational diffusion (i.e., $d>0$) on a suspension of pushers ($\alpha=-1$), without translational diffusion ($D=0$), is explored in Fig. 5. Here, the initial condition is of the form $A_{1,k}(\phi,0)=\sum_{m=1}^{M}e^{-m\beta_m}\zeta_m\sin(m\phi)$, where $\beta_m$ and $\zeta_m$ are randomly chosen and $M=20$. For $k=0.2$ and $d=0$ [Fig. 5(a) solid line], $|A_{1,k}|$ is growing, while for $k=5$ and $d=0$ [Fig. 5(b) solid line], the perturbation locks into the large $k$ oscillatory behavior. Both curves confirm the analysis of Secs. III A and III B showing growth for $k<k_1$ and oscillation in the absence of diffusion. For $k=0.2$ and $d=10^{-3}$
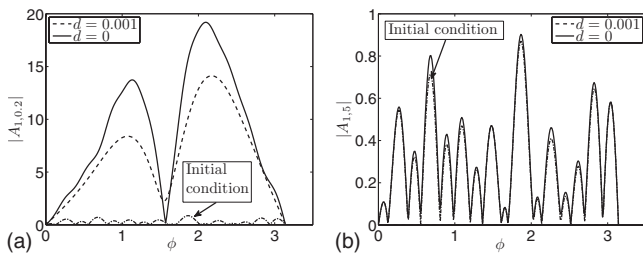


FIG. 5. Influence of rotational diffusion on $|A_{1,k}(\phi,t)|$ at $t=50$ for $\alpha=-1$ (pushers) with $D=0$ and random initial data. Differing wave numbers $k$ show growth (unstable, left) and decay (stable, right).
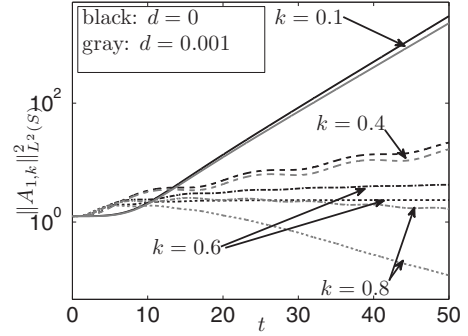


FIG. 6. Evolution of the squared $L^2(S)$ norm of the first azimuthal Fourier mode contribution to $\mathcal{S}_2$ for $\alpha=-1$ (pushers) with $D=0$. It shows the effect of rotational diffusion at differing wave numbers $k$.

[Fig. 5(a) dashed line], $|A_{1,k}|$ is growing at a smaller rate than for $d=0$. For $k=5$ [Fig. 5(b) dashed line], the solution rapidly decays.

Another way to illustrate the behavior of solutions for larger $k$ is to look at the time evolution of $\|A_{1,k}(\cdot,t)\|_{L^2(S)}^2$ (see Fig. 6). From Eq. (14), only the first $\theta$-Fourier mode can produce growth in $\mathcal{S}_2$, as all other terms are either decaying or saturating, and is thus plotted in Fig. 6, where $\alpha=-1$, $k=0.1, 0.4, 0.6, 0.8$, $D=0$, $d=0$, and $d=10^{-3}$. The initial condition is $A_{1,k}(\phi,0)=\sin(\phi)$. For $k<k_1$, $\mathcal{S}_2$ grows, a sign of the long-wave instability. For $d>0$, the contribution at $k$ large is eventually decaying as opposed to constant. If $d$ is further increased, then the $L^2(S)$ norm of every mode decays.

In order to find exponentially decaying solutions in the presence of rotational diffusion as suggested by Figs. 5 and 6, we revisit the eigenvalue problem. Again, we assume that $A_{1,k}(\phi,t)=\gamma_k(\phi)e^{\sigma t}$ in Eq. (11) and renormalize the problem so that $F[\gamma_k]=1$. Upon substitution into Eq. (11), this leads to the system

$$\gamma_k(\sigma+ik\cos\phi+Dk^2)+d\left(\frac{1}{\sin^2\phi}\gamma_k-\frac{1}{\sin\phi}\partial_\phi(\sin\phi\partial_\phi\gamma_k)\right)$$

$$=-\frac{3\alpha}{4}\cos\phi\sin\phi, \tag{28}$$

$$\int_0^\pi d\phi'\,\gamma_k(\phi',t)\sin^2\phi\cos\phi=1. \tag{29}$$

Equations (28) and (29) are solved by discretizing the $\phi$ derivatives and solving the resulting nonlinear system via Newton iteration starting from the known solution for $d=0$.

In Fig. 7, the real part of $\sigma(k)$ from Eqs. (28) and (29) with $d=0$ and $d=0.01$ is plotted. For this moderate degree of rotational diffusion, a downward shift of the branches is seen, leaving the long-wave instability intact but suppressing the lower branch. Not only does rotational diffusion reduce growth rates, it also suppresses the eigenfunction singularity seen in Fig. 2(a). In contrast to Fig. 2(a), $\gamma_k(\phi)$ is now smooth along the zero crossing of the $k$ axis and a stable branch of exponentially decaying solutions can be found for $k>k_1$.
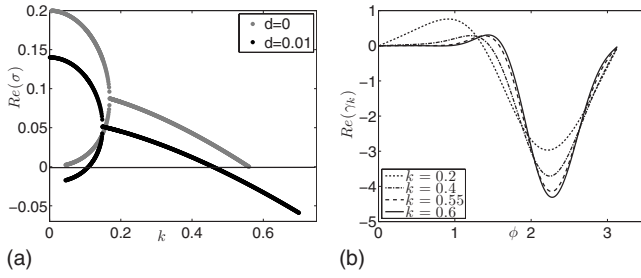
FIG. 7. For $\alpha=-1$ (pushers) and $D=0$. (Left) Continuation of the real part of the growth rate $\sigma(k)$ for positive rotational diffusion $d=0.01$. (Right) The real part of the eigenvector $\gamma_k(\phi)$ for various wave numbers $k$.

We also looked at the effect of rotational diffusion for a suspension of pullers; while the branch structure is more complex, we found no positive growth rates for $d \geq 0$, as would be expected from generic decay of the entropy. Therefore, numerical simulations confirm the analysis of Secs. III A and III B, namely, that in the absence of any diffusion, growth happens only for a finite range of wave numbers and the dynamics at small scales is controlled. Moreover, rotational diffusion reduces the strength of the long-wave instability and smooths out rapid oscillations at small scales.

## IV. COMPARISONS TO SIMULATION AND EXPERIMENT

We conclude by comparing the results of our theory to the numerical results of Saintillan and Shelley [18] and recent experiments that, in part, look at the onset of complex flow structures in motile suspensions of *B. subtilis* [25]. A simple approximation to the swimming rod model of Saintillan and Shelley gives $\alpha = \pm \pi / |\ln \epsilon^2 e|$, where $\epsilon = a/l$ is the body aspect ratio with $a$ the particle radius. For a pusher, this is found using local slender-body theory [30,31] for a swimmer that is actuated on its rear half by a constant motive tangential stress $-g_\parallel \mathbf{p}$ and with a no-slip condition on its front half. A straightforward calculation yields $U_0 = \kappa_2 l g_\parallel / \mu$, with $\kappa_2 = \epsilon |\ln \epsilon^2 e|/2$, and $\sigma_0 = -\kappa_1 l^3 g_\parallel$, with $\kappa_1 = \pi \epsilon / 2$. These determine $\alpha$ as $\alpha = \sigma_0 / U_0 \mu l^2 = -\kappa_1 / \kappa_2$. Taking $\epsilon = 0.1$ gives $\alpha \approx -0.9$, close to the value of $-1$ we have used thus far in our studies. Letting $\alpha = -1$ and neglecting diffusions, we can use the estimate derived at the end of Sec. III A to get the prediction of $\tilde{\nu} \approx 0.14$ for the critical volume concentration above which instability occurs.

However, in their simulations of rodlike swimmers, Saintillan and Shelley [18] observed that at low volume concentration (up to effective volume concentrations somewhat greater than $\tilde{\nu} = 1 = \nu/8$), the dimensional rotation diffusion $d_p$ was proportional to volume concentration $\nu$, while the dimensional translational diffusion $D_p$ was inversely proportional. That is, $d_p \approx \nu \bar{d}_p$ and $D_p \approx \nu^{-1} \bar{D}_p$. They conjectured that orientational dispersion resulted mostly from pair interactions, giving the linear dependence of $d_p$ upon $\nu$, while center-of-mass dispersion was consistent with Brenner's generalized Taylor dispersion analysis [32] where $D_p = U_0^2 / (6 d_r)$. In their force dipole simulations, Hernández-
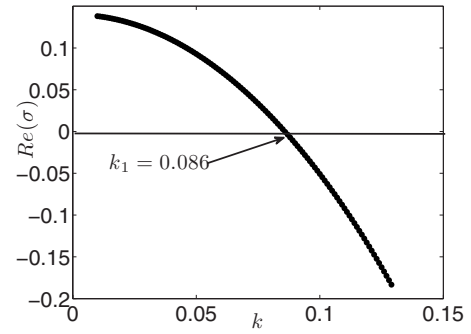


FIG. 8. Crossing of the upper branch of computed growth rates from positive to negative with increasing $k$. Here, the diffusion coefficients, $d=0.01$ and $D=16.67$, are taken from Saintillan and Shelley [18].

Ortiz *et al.* also found a decrease in the translational diffusion coefficient with volume concentration, albeit a slower one. Recall that Eqs. (1)–(5) are scaled on velocity $U_0$ and intrinsic length $l_c = \nu^{-1} l$. If one assumes the observed scalings of $d_p$ and $D_p$ with $\nu$, the adimensional diffusion coefficients become

$$ d = \frac{l \bar{d}_p}{U_0} \quad \text{and} \quad D = \frac{\bar{D}_p}{l U_0}. $$

That is, $d$ and $D$ depend only on swimmer speed and length, while system size and swimmer volume concentration appear only in the normalized system size $L = L_p / l_c$ and hence in the normalized wave number $k = (2\pi l)/(\nu L_p)k'$.

Using the numerical values for $\bar{d}_p$ and $\bar{D}_p$ gleaned from Saintillan and Shelley [18], we solve the eigenvalue problem in Eqs. (28) and (29) and plot in Fig. 8 the growth rate $\mathrm{Re}(\sigma)$ as a function of $k$. This yields the crossing value $k_1 \approx 0.086$ and hence instability is found if $k_1' = (k_1/2\pi)(\nu L_p/l) > 1$. Taking $l=1$ and $L_p=10$ (as in [18]), the figure predicts the existence of a critical volume concentration, $\tilde{\nu} = 0.9$ as defined by Saintillan and Shelley ($\tilde{\nu} = \nu/8$) for the emergence of a long-wave instability. This is consistent with their result that organized dynamics emerges at volume concentrations in the neighborhood of $\tilde{\nu} = 0.5$ [[38]; also, see Fig. 2(b) of [18]].

This analysis alternatively predicts, for fixed $\nu$, a critical system size above which a pusher suspension is unstable and below which it is stable. Recent experiments of Sokolov *et al.* [25] investigated the dynamics of motile *B. subtilis* suspended in free-standing water films. They find, among other things, a transition from what they describe as a state of essentially two-dimensional collective swimming to one with fully three-dimensional complex dynamics. This transition occurs as film thickness is increased and, in particular, for number concentrations of $n \approx 2.5 \times 10^{-2}$ $\mu m^{-3}$, they report a critical film thickness of $L_p \approx 200$ $\mu m$. They also report that at film thicknesses less than 100 $\mu m$, the bacterial concentration is nearly uniform with some slight depletion in the center. Plainly, this observed transition is from a different base state (two-dimensional collective dynamics) than that studied here (isotropic and uniform) and their experiment is complicated by bacterial taxis, possibly oxygen mediated,

toward the free surfaces as well as by gravitational effects. Further, in these experiments, the bacterial concentrations are quite high ($\tilde{\nu} \approx 2$) and perhaps out of the range of validity of our theory. Our analyses—using either a stability threshold calculated in the absence of diffusive effects or using the relation used for comparison to Saintillan and Shelley—predict critical length scales considerably smaller, on the order of 50 $\mu$m or less.

## V. CONCLUSION

In this work, we used a kinetic model [19,20] to investigate the stability of suspensions driven by the active swimming of particles. We analyzed the generalized linear problem about an isotropic and uniform state. As previously shown by Saintillan and Shelley [19,20], the eigenvalue problem shows that in the case of pushers, fluctuations at long scales are exponentially amplifying. Additionally, we find that in the absence of any diffusion, short-scale perturbations lock into an oscillatory behavior, set by the initial condition, independently of the swimming mode. In particular, a small wavelength analysis, as well as numerical simulation, shows that the contribution resulting from the active extra stress decays to zero in time. While concentration fluctuations are generically bounded in the linear stability analysis, numerical simulations of Saintillan and Shelley [19,20] show that large-amplitude nonlinear flow structures are associated with concentration fluctuations and hence are not captured by the present study. We also investigate the effect of rotational diffusion and find, as expected, that it reduces growth at long waves and also allows the existence of eigenvalues past the zero growth-rate boundary. Furthermore, if rotational diffusion scales with swimmer concentration and translational diffusion inversely, then we predict a critical volume concentration or system size characterizing the onset of the long-wave instability. This analysis gives a reasonable accounting of the particle simulations of Saintillan and Shelley [18] and a less satisfactory one for the experiments of Sokolov *et al.* [25], though the experiments are complicated by other factors, as discussed.

This study is an attempt at understanding the stability of suspensions of active swimmers and the structure of their mathematical characterizations. With respect to the kinetic theory, it would be interesting to study the more general stability of perturbations about an evolving state. Further, our analysis is an approximate one and these systems await a rigorous analysis approach to stability and well-posedness (as in [33] for rigid rod suspensions). We found it interesting that the stability problem could be wholly reduced to the dynamics of the first azimuthal mode.

The kinetic model is itself an idealization. For example, it is a dilute theory that does not capture close or steric interactions that may be important in determining the emergence of collective swimming states [39]. Near body interactions of two swimmers have been studied theoretically and numerically by Ishikawa *et al.* [34] among others for squirming spheres with prescribed tangential velocities. These hydrodynamic effects lead to complex dynamics (attraction, repulsion) in the near field, but do not change the dipolar far-field flow structure. Hydrodynamics of nearby swimmers was also considered theoretically by Pooley and co-workers [35,36] for the three-linked sphere model of Najafi-Golestanian [37], whose net displacement is achieved via a periodic and time-irreversible motions. They found a similar complicated local dynamics (attractive, repulsive, or oscillatory) and further showed that the time-averaged dipolar contribution to the far-field flow disappears. While both of these studies are perhaps relevant in understanding collective swimming, they are beyond the scope of this work which is a dilute theory with a dipolar far-field flow.

These studies do raise the question of what extensions the theory can accommodate. For example, consider cyclic swimmers such as *Chlamydomonas* whose two pulling flagella are expected to produce a temporally modulated stress dipole of positive average strength (a puller). If the relative temporal phase of the swimming stroke is introduced as a configuration variable, with each swimmer having an independent phase (i.e., asynchronous swimming, perhaps consistent with far-field interactions), then the distributional average over phase for the macroscale extra stress will eliminate any dependence on phase and renormalize the term's coefficient. Similarly, the single-particle flux will be modified and then renormalized by a distributional average. Moreover, the present study only considers rodlike swimmers, where the shape parameter $\gamma$, in a generalized Jeffrey's equation [see Eq. (3) in [19]], equals 1. Following Saintillan and Shelley [19], it can been seen that the introduction of $\gamma$ is equivalent to replacing $\alpha$ by $\alpha\gamma$. Therefore, nearly spherical ($\gamma \approx 0$) pullers such as *Chlamydomonas* are not expected to show instabilities away from the isotropic state, even were they pushers. Our analysis is also restricted to spatially periodic states and perturbations, and boundaries and boundary conditions are undoubtedly determinants of stability. Finally, recent experimental observations [9] have motivated theoretical work [11] on the hydrodynamics of single magnetically driven microswimmers. The stability of clouds of such swimmers, in which there will be interacting hydrodynamic and magnetic couplings, is a very interesting question.

[1] C. Brennen and H. Winet, Annu. Rev. Fluid Mech. **9**, 339 (1977).

[2] J. Gray and G. Hancock, J. Exp. Biol. **32**, 802 (1955).

[3] E. Gouin, M. D. Welch, and P. Cossart, Curr. Opin. Microbiol. **8**, 35 (2005).

[4] A. M. Leshansky, Phys. Rev. E **74**, 012901 (2006).

[5] W. F. Paxton, K. C. Kistler, C. C. Olmeda, A. Sen, S. K. St. Angelo, Y. Cao, T. E. Mallouk, P. E. Lammert, and V. H. Crespi, J. Am. Chem. Soc. **126**, 13424 (2004).

[6] R. Golestanian, T. B. Liverpool, and A. Ajdari, Phys. Rev. Lett. **94**, 220801 (2005).

[7] J. R. Howse, R. A. L. Jones, A. J. Ryan, T. Gough, R. Vafaba-khsh, and R. Golestanian, Phys. Rev. Lett. **99**, 048102 (2007).

[8] R. Dreyfus, J. Baudry, M. L. Roper, H. A. Stone, M. Fer-migier, and J. Bibette, Nature (London) **437**, 862 (2005).

[9] D. Zerrouki, J. Baudry, D. Pine, P. Chaikin, and J. Bibette, Nature (London) **455**, 380 (2008).

[10] E. E. Keaveny and M. R. Maxey, J. Fluid Mech. **598**, 293 (2008).

[11] E. E. Keaveny and M. J. Shelley, Phys. Rev. E **79**, 051405 (2009).

[12] I. Tuval, L. Cisneros, C. Dombrowski, C. W. Wolgemuth, J. O. Kessler, and R. E. Goldstein, Proc. Natl. Acad. Sci. U.S.A. **102**, 2277 (2005).

[13] C. Dombrowski, L. Cisneros, S. Chatkaew, R. E. Goldstein, and J. O. Kessler, Phys. Rev. Lett. **93**, 098103 (2004).

[14] L. H. Cisneros, R. Cortez, C. Dombrowski, R. E. Goldstein, and J. O. Kessler, Exp. Fluids **43**, 737 (2007).

[15] A. Sokolov, I. S. Aranson, J. O. Kessler, and R. E. Goldstein, Phys. Rev. Lett. **98**, 158102 (2007).

[16] J. P. Hernández-Ortiz, C. G. Stoltz, and M. D. Graham, Phys. Rev. Lett. **95**, 204501 (2005).

[17] P. T. Underhill, J. P. Hernandez-Ortiz, and M. D. Graham, Phys. Rev. Lett. **100**, 248101 (2008).

[18] D. Saintillan and M. J. Shelley, Phys. Rev. Lett. **99**, 058102 (2007).

[19] D. Saintillan and M. J. Shelley, Phys. Rev. Lett. **100**, 178103 (2008).

[20] D. Saintillan and M. J. Shelley, Phys. Fluids **20**, 123304 (2008).

[21] M. Doi and S. Edwards, *The Theory of Polymer Dynamics* (Oxford University Press, New York, 1986).

[22] R. A. Simha and S. Ramaswamy, Phys. Rev. Lett. **89**, 058101 (2002).

[23] A. Baskaran and M. C. Marchetti, Proc. Natl. Acad. Sci. U.S.A. **106**, 15567 (2009).

[24] G. Subramanian and D. L. Koch, J. Fluid Mech. **632**, 359 (2009).

[25] A. Sokolov, R. E. Goldstein, F. I. Feldchtein, and I. S. Aranson, Phys. Rev. E **80**, 031903 (2009).

[26] T. Ishikawa and T. J. Pedley, J. Fluid Mech. **588**, 399 (2007).

[27] A. Kanevsky, M. J. Shelley, and A. K. Tornberg, J. Comput. Phys. **229**, 958 (2010).

[28] J. B. Jeffery, Proc. R. Soc. London, Ser. A **102**, 161 (1922).

[29] G. K. Batchelor, J. Fluid Mech. **46**, 813 (1971).

[30] J. B. Keller and S. I. Rubinow, J. Fluid Mech. **75**, 705 (1976).

[31] A. K. Tornberg and M. Shelley, J. Comput. Phys. **196**, 8 (2004).

[32] H. Brenner, J. Colloid Interface Sci. **71**, 189 (1979).

[33] F. Otto and A. E. Tzavaras, Commun. Math. Phys. **277**, 729 (2008).

[34] T. Ishikawa, M. P. Simmonds, and T. J. Pedley, J. Fluid Mech. **568**, 119 (2006).

[35] C. M. Pooley, G. P. Alexander, and J. M. Yeomans, Phys. Rev. Lett. **99**, 228103 (2007).

[36] G. P. Alexander, C. M. Pooley, and J. M. Yeomans, J. Phys.: Condens. Matter **21**, 204108 (2009).

[37] A. Najafi and R. Golestanian, Phys. Rev. E **69**, 062901 (2004).

[38] D. Saintillan (private communication).

[39] I. Aranson (private communication).